REPRINTED FROM:

JIST

JOURNAL OF IMAGING SCIENCE AND TECHNOLOGY

VOL. 66, NO. 6 / NOVEMBER/DECEMBER 2022

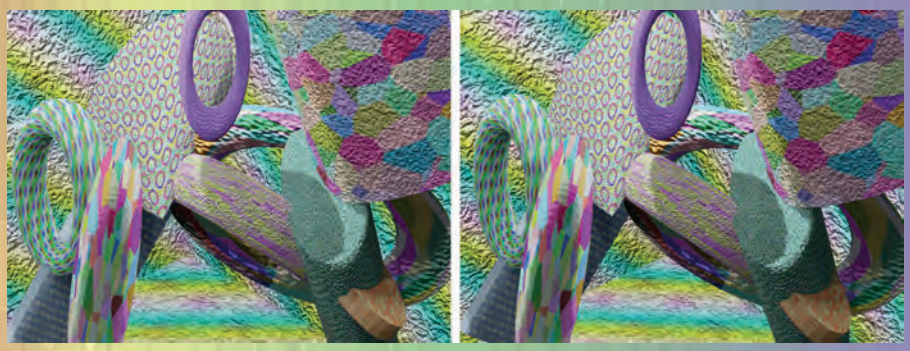

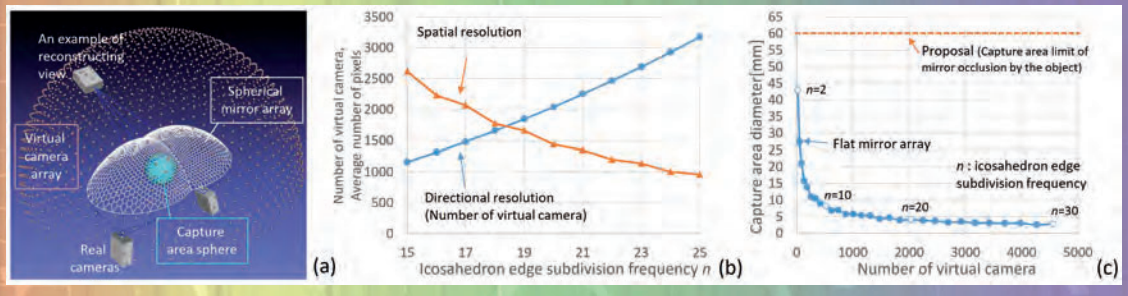

IS&T
imaging.org

Journal of Imaging Science and Technology® 66(6): 060404-1–060404-11, 2022.

Structure-Aware Color Halftoning with Adaptive Sharpness Control

Fereshteh Abedini▲ and Sasan Gooran▲
Linköping University, Media and Information Technology Division, Department of Science and Technology, Norra Grytsgatan 10, Norrköping, Sweden, 60233
E-mail: fereshteh.abedini@liu.se

Abstract. *Structure-aware halftoning algorithms aim at improving their non-structure-aware version by preserving high-frequency details, structures, and tones and by employing additional information from the input image content. The recently proposed achromatic structure-aware Iterative Method Controlling the Dot Placement (IMCDP) halftoning algorithm uses the angle of the dominant line in each pixel's neighborhood as supplementary information to align halftone structures with the dominant orientation in each region and results in sharper halftones, gives a more three-dimensional impression, and improves the structural similarity and tone preservation. However, this method is developed only for monochrome halftoning, the degree of sharpness enhancement is constant for the entire image, and the algorithm is prohibitively expensive for large images. In this paper, we present a faster and more flexible approach for representing the image structure using a Gabor-based orientation extraction technique which improves the computational performance of the structure-aware IMCDP by an order of magnitude while improving the visual qualities. In addition, we extended the method to color halftoning and studied the impact of orientation information in different color channels on improving sharpness enhancement, preserving structural similarity, and decreasing color reproduction error. Furthermore, we propose a dynamic sharpness enhancement approach, which adaptively varies the local sharpness of the halftone image based on different textures across the image. Our contributions in the present work enable the algorithm to adaptively work on large images with multiple regions and different textures.* © *2022 Society for Imaging Science and Technology.*
[DOI: 10.2352/J.ImagingSci.Technol.2022.66.6.060404]

1. INTRODUCTION

Image reproduction devices such as printers are binary tools that can only choose to place a dot at a particular position of a substrate using only a limited number of inks [1]. Digital halftoning is the process of converting a continuous-tone image into a binary image for printing purposes. Halftoning algorithms are divided into three main categories: thresholding and table halftoning [2], error diffusion [3–7], and iterative [8–11] methods. Thresholding and non-modified error diffusion are simple techniques, but they introduce different types of artefacts that worsen the representation of the original image. However, iterative methods such as the Direct Binary Search (DBS) [8] and the Iterative Method Controlling the Dot Placement (IMCDP) [9] create higher halftone quality at the cost of computational complexity.

Color printers use four primary colorants, typically cyan, magenta, yellow, and black (CMYK). In addition to the four primary colors, multi-channel or High-Fidelity (HiFi) printing uses extra inks to improve the quality of color printing. Color halftoning converts a continuous-tone color image into binary images for each ink. One simple, yet efficient, approach for color halftoning is to apply achromatic halftoning algorithms to different color channels independently. The final color halftoned image is then retrieved by superposition of all the monochrome halftoned images.

Halftoning techniques have gone through different improvements by supplementing the halftoning algorithm with supplemental information about the original image content to better preserve tonal and structural resemblance to the original continuous-tone input image [12–21]. As these techniques are aware of details and structures of the original image, they are referred to as structure-aware or structure-based halftoning.

In this paper, we introduce an adaptive structure-aware color halftoning algorithm based on the CMY colorant channels. It is an extension of the IMCDP halftoning algorithm, which reproduces well-formed halftone structures with the possibility of changing the halftone's shape and structure. The achromatic structure-aware IMCDP was recently proposed as a structure-aware halftoning algorithm that improves the sharpness of the halftone image and simultaneously better preserves the tone and structure similarity compared to the original IMCDP [21]. However, the preprocessing step of the algorithm was slow, and it has been applied only to monochrome images. In this paper, (1) we review the approach in the preprocessing step and propose a faster and more flexible technique for obtaining the local orientation in structure-aware IMCDP, (2) extend the algorithm to color halftoning, and (3) improve its performance by introducing an adaptive approach to adjust the degree of sharpness enhancement in a spatial varying manner across the image.

2. RELATED WORK

A high-quality halftone should present faithful reproduction of the tonal and structural content of the original image.

▲ IS&T Members.

Received June 30, 2022; accepted for publication Nov. 10, 2022; published online Dec. 5, 2022. Associate Editor: Kye Si Kwon.
1062-3701/2022/66(6)/060404/11/$25.00

As structures may be lost during halftoning, the halftone image sometimes fails to truly represent the structures and tones of the continuous-tone original image. Structure-aware (structure-based) halftoning methods have been developed with the aim of better preserving tonal and structural details by feeding the important content of the original image as an additional input to the halftoning process. For instance, Eschbach and Knox used the inverse of input image as a threshold in the halftoning process and enhanced edge reproduction in error diffusion [13]. Chang et al. used the main component of local frequency in the original image as lookup table indices to modify the error-diffusion coefficients and improved the visual quality of halftones [15]. Liu et al. proposed an entropy-based method that measures the intensity's impact and adaptively modifies the threshold's constraints in the halftoning algorithm [16]. Pang et al. defined an objective function, measuring tone and structure similarity between the original image and the halftone image. By optimizing the objective metric, the algorithm generates images, which preserve texture details and local tone faithfully [14]. Li and Mould employed the contrast information of the original image and generated a contrast-aware mask for diffusing the error to neighborhood's pixels in error diffusion halftoning [12]. Li et al. also used the error diffusion halftoning algorithm as the underlying method and employed the intensity of edges in the original image to calculate the texture information. They used the texture information as a mask to better diffuse the error to pixels [20]. Abedini et al. used the local orientations of the original image to align the halftone structure with the dominant line in each neighborhood. Their proposed structure-aware halftoning reproduces sharper halftones, while better preserves tonal and structural similarities compared to its non-structure-aware version [21]. Not all the proposed structure-aware halftoning methods have been tested on color images. Some researchers have extended their proposed method to color halftoning by applying their achromatic halftoning algorithm independently on different colorant channels; however, they have not studied the effect of separate monochromatic halftoning on final results [12, 14, 16, 20].

In this paper, we aim to improve the recently proposed monochromatic structure-aware IMCDP [21] by introducing a faster and more stable approach for extracting the local orientations, extend it to color halftoning by investigating the effect of running an independent or dependent halftoning over each colorant channel, and improve its flexibility by proposing an adaptive sharpness enhancement across the image.

3. METHOD

In our previous work, we used the local orientation of pixels to develop a structure-aware halftoning method based on IMCDP [21]. It has been shown that the structure-aware version of the IMCDP reproduces sharper halftones and better preserves the tone and structure similarity of the input image. However, the method presented in Ref. [21] is only developed for monochrome halftoning and the degree of sharpness enhancement is constant for the entire image.

The contributions of this paper are: (1) using a faster and more flexible approach for obtaining the orientation in the preprocessing step, (2) extending the structure-aware IMCDP to color halftoning, and (3) using adaptive sharpness enhancement across the image. These contributions enable the algorithm to work on large and diverse images that have multiple regions with different textures. In Section 3.1, we briefly review the monochrome structure-aware IMCDP, and we elaborate on our proposed method for improving the structure-aware IMCDP in Section 3.2.

3.1 *Monochrome Structure-Aware IMCDP*

The key idea of the monochrome structure-aware IMCDP is to align the dot placement along edges and textures of the image. Our goal was to improve the reproduction of high-frequency details while preserving the tonal and structural resemblance to the original image. We developed the method based on the IMCDP halftoning algorithm [9] and used the Hough transform [22] to extract local orientation information.

IMCDP is an iterative halftoning algorithm, which starts with a blank image the same size as the original image (to be the halftone image). The algorithm searches for the pixel holding the maximum value in the continuous-tone image, and the first dot is placed at its corresponding position in the blank halftone image. To consider the effect of this quantization, the low-pass filtered version of the halftone image is subtracted from the low-pass filtered version of the original image. This process is called feed-back process, and, accordingly, the filter is referred to as feed-back filter. The algorithm continues with finding the next pixel holding the highest value after subtracting the filtered halftone image. Because the average tone value in different gray-tone regions in the halftone image should be the same as the original image, the total number of black dots to be placed in each tonal region is known in advance, so the algorithm terminates when the predetermined number of black dots is placed in the halftone image [9].

One important point about IMCDP is the shape of the feed-back filter. In the original IMCDP, a symmetrical Gaussian kernel, as defined in Eq. (1) is used in the feed-back process. As a result, the dots are placed symmetrically in all directions. However, using a nonsymmetrical Gaussian kernel, as in Eq. (2), makes the distribution of dots nonsymmetrical [23].

$$f(x,y) = Ke^{-\left(\frac{x^2+y^2}{2\sigma^2}\right)} \tag{1}$$

$$f(x,y) = Ke^{-(Ax^2+2Bxy+Cy^2)}, \tag{2}$$

where, (x, y) are the spatial coordinates of pixels, K is a normalization factor to ensure that the filter elements sum to 1, σ is the standard deviation of the Gaussian kernel, and

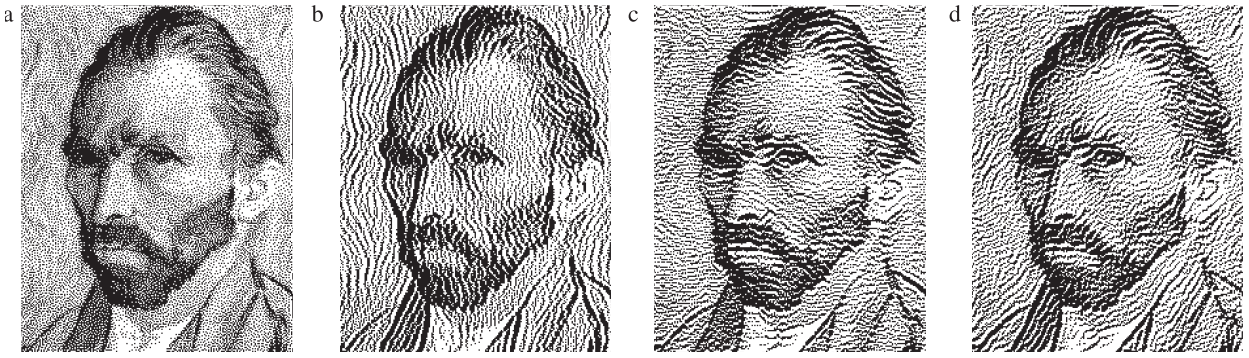

Figure 1. Grayscale image being halftoned using; (a) a symmetrical filter as in Eq. (1) in the feed-back process; (b) a nonsymmetrical filter of the form as in Eq. (2) in the feed-back process with vertical alignment $k_1 = 3, k_2 = 1, \varphi = 0°$; (c) a nonsymmetrical filter of the form as in Eq. (2) in the feed-back process with horizontal alignment $k_1 = 1, k_2 = 3, \varphi = 0°$; (d) a nonsymmetrical filter of the form as in Eq. (2) in the feed-back process with horizontal alignment $k_1 = 1, k_2 = 3$, rotated by $\varphi = 30°$. Halftone images are displayed at 150 dpi. This figure is best viewed in the electronic version of this paper.

constants A, B, and C are calculated as:

$$A = \frac{\cos^2\varphi}{2k_1\sigma^2} + \frac{\sin^2\varphi}{2k_2\sigma^2}, \tag{3}$$

$$B = \frac{-\sin 2\varphi}{4k_1\sigma^2} + \frac{\sin 2\varphi}{4k_2\sigma^2}, \tag{4}$$

$$C = \frac{\sin^2\varphi}{2k_1\sigma^2} + \frac{\cos^2\varphi}{2k_2\sigma^2}. \tag{5}$$

Parameters k_1 and k_2 in the nonsymmetrical kernel are used to adjust the shape of the halftone structure. Setting $k_1 = k_2$ creates symmetrical halftones, while $k_1 > k_2$ makes halftones grow faster in vertical direction, resulting in vertical line-halftones, and conversely, $k_1 < k_2$ generates halftones with horizontal alignments, resulting in horizontal line-halftones. Figure 1 shows a visual example of flexibility of IMCDP in generating different halftone structures by using different Gaussian kernels in the feed-back process.

Different halftone structures, produced by the IMCDP, could be combined in the same image with smooth transition [24]. The flexibility of IMCDP in generating line-halftone structures makes it a powerful algorithm to adaptively change the halftone structure according to the image content. In the monochrome structure-aware IMCDP, we used the Hough transform to detect the dominant line in the neighborhood of each pixel [21]. As a result, the input image is divided into structured (union of pixels with a dominant line or sharp edge in their neighborhood) and structureless regions (union of pixels with no line in their neighborhood). Then, different halftone structures have been used based on the orientation of the dominant line. To be more specific, at pixels lying in the structureless region, a symmetrical Gaussian filter with the form of Eq. (1) is used as the feedback filter, while at pixels with a line in their neighborhood a nonsymmetrical Gaussian filter with the form of Eq. (2) is applied.

To align halftones with the dominant line in the neighborhood of a pixel, we made horizontal halftone ($k_1 < k_2$) and rotated it by setting the angle (φ) to the angle of the dominant line. This means that the halftone structure is aligned with the dominant line in the pixel's neighborhood. Therefore, the edge information is more emphasized, and the halftone image preserves more details at edges. Figure 2 illustrates the workflow of developing the recently proposed structure-aware IMCDP [21]. It was found that generating horizontal halftone line by setting parameters k_1 and k_2 to 1 and 1.8, respectively, and setting the angle φ to the angle of the dominant line in the structure-aware IMCDP results in sharper halftones while better preserves the tonal and structural similarity compared to the original IMCDP.

3.2 *Color Structure-Aware IMCDP*

In Ref. [21], the Hough transform was used to detect the dominant line in the neighborhood of each pixel in the input image, and partition the image into structured and structureless regions. The angle of the dominant line was then calculated, and a nonsymmetrical Gaussian kernel was applied based on its orientation in the feedback process in structured regions and a symmetrical Gaussian kernel in structureless regions. This approach has two main limitations:

- The Hough transform based preprocessing can be prohibitively expensive as it has cubic complexity.
- Relative sharpness enhancement is static across the entire structured regions of the image.

In this paper, we address both these limitations, and extend the method to color halftoning.

3.2.1 *A Faster preprocessing Approach to Calculate the Local Orientation*

In the preprocessing step, a fast and stable approach to estimate the local orientations of an image is needed. We require the method to have at most quadratic complexity since it is the best-case complexity imposed by the nature of IMCDP. We reviewed approaches based on local image gradient and Gabor responses at different scales. They both have the same time complexity; however, we observed that the Gabor-based approach is more robust.

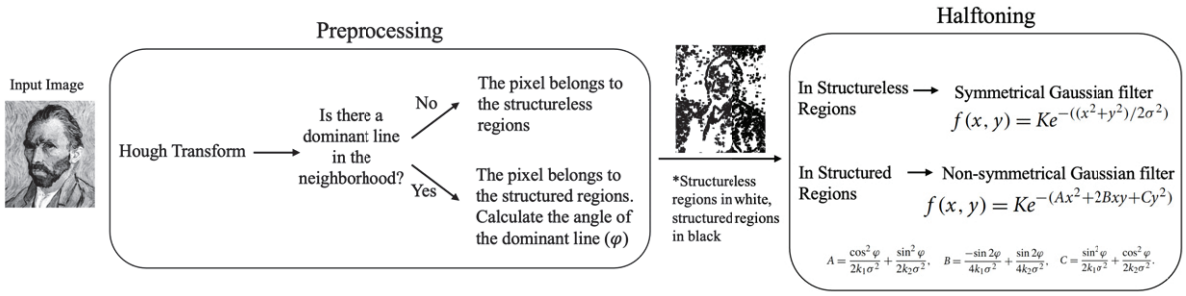

Figure 2. Workflow of developing the monochrome structure-aware IMCDP.

Gabor filter captures local frequency and direction of an image and is extensively used in texture analysis [25]. The image is convoluted with a set of filters called Gabor filter bank. Each filter is characterized by its wavelength (λ), orientation (θ), bandwidth (σ), phase offset (ψ), and aspect ratio (γ). Intuitively, each Gabor filter is a Gaussian kernel function modulated by a sinusoidal plane wave, where the Gaussian component provides the weights, and the sinusoidal component provides the directionality. One constructs a Gabor filter bank with several parameters and infers the local texture characteristics of the image from its response to the filters. Refer to [26] for a detailed explanation of the use of Gabor filter. In this work, we used a bank of 36 Gabor filters at equally distanced orientation in $\theta = [0°, 180°)$ with constant wavelength $\lambda = 20$, $\sigma = 1$, $\psi = 0$, and $\gamma = 0.5$. We calculated the response of Gabor filters at those 36 directions and the direction with the largest magnitude of response is considered the dominant orientation at each pixel.

3.2.2 *Extending to Color Halftoning*

Color printers use four different colorants, typically CMYK. In addition to these four primary colors, some printers, referred to as multi-channel or HiFi printers, use more inks to reproduce more of the color spectrum. One simple, yet efficient, approach for color halftoning is to apply the monochrome halftoning algorithms to different color channels independently and retrieve the final color halftone image by the superposition of all the monochrome halftone images.

In this work, to apply the proposed method to color images, we convert the RGB continuous-tone image to three colorant channels: $C = 1 - R$, $M = 1 - G$, and $Y = 1 - B$, we extract the orientation information in each channel independently and run our monochrome structure-aware IMCDP over C, M, and Y channels, separately. To consider four-color printers (C, M, Y, K), we assume that full under-color removal is employed. It means that at a given position, a black dot is placed, if and only if all three channels are present [27]. Note that the conversion from RGB to CMY depends on the physical process being used to lay down the CMY ink; therefore, there are several methods to transform an RGB image to CMY color channels. For instance, in Ref. [28], Shaked et al. proposed a different approach to initialize CMYK for color error diffusion halftoning.

In this paper, we illustrate our approach to extend the monochromatic structure-aware IMCDP to color halftoning based on C, M, Y channels; however our proposed structure-aware color halftoning is not limited to CMYK printers. Because the input color image is first converted to different channels and the method is applied on each channel separately, our approach could also be employed by printers which use extra inks.

Extracting orientation information for three colorant channels separately is computationally expensive. One possible approach is to derive the orientation information from the luminance channel and use the same angle information for three colorant channels C, M, and Y. To study if the luminance orientation is a good approximation of color channels' orientation, we derived the luminance component of each RGB input image using Eq. (6) and used its orientation information for all three colorant channels. The coefficients used in Eq. (6) are identical to those used to calculate luminance in Ref. [29]. The impact of this simplification on the algorithm is discussed in Section 5.

$$\text{Luminance component} = 0.289R + 0.587G + 0.114B. \quad (6)$$

3.2.3 *Adjusting Sharpness Enhancement*

In the original structure-aware IMCDP, the sharpness enhancement was static throughout the structured regions with fixed values of $k_1 = 1$ and $k_2 = 1.8$. Although a fixed sharpness enhancement produces acceptable results, it may not produce optimal results, especially for images that have multiple objects or areas with different textures. We propose an approach where the relative degree of sharpness enhancement is defined for each pixel of the image with variable k values. Without loss of generality, we assume $k_1 = 1$ and calculate a variable k_2 for each pixel of the image. We use the Gabor filters described in Section 3.2.1 to analyze the texture of the image to infer the degree of local image sharpness. Intuitively, in a sharp area of an image, such as at an edge, we expect a high response from the Gabor filter that is aligned with the edge and low response in other directions. On the other hand, in an area with no edge or other significant feature, we expect relatively similar responses from Gabor filters of all orientations.

We use the ratio between the maximum Gabor response to the average of the responses for each point as a representation of local image sharpness. For a bank of n Gabor filters, and $G = [g_1, g_2, \ldots, g_n]$ responses to those n filters, we define local sharpness at each pixel as:

$$s = \frac{\max(G)}{\text{mean}(G)} \quad \text{for } G = [g_1, g_2, \ldots, g_n]. \tag{7}$$

Calculated ratio of local sharpness, s, needs to be transferred to an appropriate value for k_2 in IMCDP. Since the calculated local sharpness changes with color, brightness, and other features for different images, we calculate the transformation from local sharpness, s, to k_2 empirically for each input image. For each input image, we generate two reference images, one random white noise (reference image W) and one sinusoidal image with wavelength similar to the Gabor filters (reference image S), both with the same dynamic range as the original image. The n Gabor filters are applied to the images S and W to produce $G^{(s)}$ and $G^{(W)}$ at each pixel and then using Eq. (7), the local sharpness value for two reference images is calculated as $s^{(S)}$ and $s^{(W)}$. The random noise should produce the local sharpness values (s) corresponding to $k_2 = 1$, and the sinusoidal image should produce local sharpness values corresponding to $k_2 = \max_{k_2}$. The inferred k_2 for each pixel is then calculated as a linear interpolation between these two values and capped at $\max_{k_2}$ using Eq. (8):

$$k_2 = \max\left(\frac{s - S^{(W)}}{S^{(S)} - S^{(W)}} \max_{k_2}, \max_{k_2}\right), \tag{8}$$

where s is the sharpness value at each pixel of the input image (calculated by Eq. (7)), $\max_{k_2}$ is a hyperparameter of the proposed algorithm, $S^{(S)}$ and $S^{(W)}$ are the average of $s^{(S)}$ and $s^{(W)}$, respectively. The effect of the variable k_2 on halftoning is studied in Section 5.

4. EVALUATION APPROACH

The goal of this paper is to improve the recently proposed monochrome structure-aware IMCDP halftoning algorithm to use a faster and more flexible approach for obtaining the angle in the preprocessing step, extend it to color halftoning, and apply a dynamic sharpness enhancement ratio across the image. We study the impact of the proposed improvements on the performance of the structure-aware color halftoning by assessing sharpness, structure similarity, color consistency, and computation time.

4.1 *Perceptual Aspects*

To evaluate a halftoning algorithm and compare the halftone image with the continuous-tone color version of it, it is important to consider the human visual system (HVS) characteristics. Human visual system creates an illusion of a continuous-tone image when the halftone image is viewed from a sufficiently large distance. The decrease in sensitivity (blurring effect) that occurs in the HVS increases as a function of cycles-per-degree of visual angle. Visual angle is a function of resolution and viewing distance, and it is calculated as in Eq. (9):

$$\text{Visual Angle} = \frac{R}{\frac{180}{\pi}\tan^{-1}\left(\frac{1}{D}\right)} \text{cycles/degree}. \tag{9}$$

In Eq. (9), R defines the resolution in *dpi* or *ppi* and D is the viewing distance in inches.

Different methods have been proposed to model the blurring effect of the HVS and the contrast sensitivity function (CSF) [2, 30–33]. The CSF describes the sensitivity of the HVS to different spatial and temporal frequencies that are present in the visual stimulus.

Because the halftone and the continuous-tone image are viewed at different resolutions, we use two different visual angles to properly simulate the function of the HVS. According to Eq. (9), to simulate a continuous-tone image, being viewed at a typical display of 100 ppi from a distance of 11.8 inches (30 cm), the visual angle would be 20.6 cycles/degree. However, to simulate the contrast sensitivity function of HVS for a halftone image, printed with a typical high-quality printer, at a resolution of 600 dpi and being viewed from distance of 13 inches (33 cm), the visual angle is 136.4 cycles/degree. In all the evaluations in this paper, to account for the HVS functionality, the halftone and the original image have been processed by visual angles of 136.4 and 20.6 cycles/degree, respectively. We perform the proposed color structure-aware IMCDP halftoning algorithm in CMY color space, but we evaluate the results in RGB space. The reason is that our HVS is modeled in RGB space [14].

4.2 *Evaluation Metrics*

We evaluate our proposed method by studying three important aspects in image reproduction process: improving generating high-frequency contents, better preserving the structures and details, and faithful color reproduction of the original image.

4.2.1 *Sharpness*

To quantify the performance of the proposed algorithm in generating details, we find the no-reference perceptual blur metric proposed by Crete et al. practical for our study [34]. Their blur metric is estimated only on the luminance component and based on the discrimination between different levels of perceptible blur. Crete et al. quantified the final blur metric value in the range of 0 to 1, corresponding to the sharpest and blurriest perception, respectively. A lower blur metric corresponds to better reproduction of the high-frequency details in a halftone image; thus, the halftone structure has less blur annoyance and is considered as more pleasant to the human eye.

4.2.2 *Structure Similarity*

The halftone image should appear visually similar to the original (input) image being viewed from an appropriate distance. We use the structural similarity index measure (SSIM) proposed by Wang et al. to evaluate the structural

similarity between images [35]. Here, we compute the mean SSIMs (MSSIM) over blocks of size $L \times L$ ($L = 11$) for evaluating the structure similarity of results. The valid range for the MSSIM is from 0 to 1, a higher value corresponds to a higher similarity. The original quality assessment metric MSSIM has been applied only to the luminance component of the image. According to Wang et al., even though their experiments showed that the use of the other color components did not significantly change the performance of the metric, this should not be considered generally true for color image quality assessment. Therefore, we used the color version of MSSIM as Eq. (10) by running it over R, G, B channels separately, and compared the results to the MSSIM values using only the luminance component.

$$MSSIM = \frac{1}{3}(MSSIM_R + MSSIM_G + MSSIM_B). \quad (10)$$

As with Wang et al.., we did not find a significant difference in the performance of the metric using the other color components of images therefore, we use the luminance component of images to compute the MSSIM reported in Section 5.

4.2.3 *Color Consistency*

To measure the perceived color difference between the halftone and continuous-tone image, we use the Spatial CIELAB (S-CIELAB) metric proposed by Zhang et al. [33]. S-CIELAB is a spatial extension of CIELAB, based on an opponent-channel-representation-based HVS model to predict the perceived quality of color halftone images. S-CIELAB computes the perceived color difference as follows. First, the CIEXYZ representation of a color image is transformed to the opponent color space (Luminance, Red–Green, and Blue–Yellow). Next, the data in each color channel is convolved by a two-dimensional spatial kernel of the form of a series of Gaussian functions, simulating the visual spatial sensitivity of the HVS to the corresponding color dimension, as:

$$f(x, y) = k \sum_i w_i E_i(x, y), \quad (11)$$

where,

$$E_i(x, y) = k_i \exp\left(-\frac{x^2 + y^2}{\sigma_i}\right). \quad (12)$$

The parameters k and k_i normalize the filters such that they sum to one. The parameters w_i and σ_i represent the weight and standard deviation of the Gaussian kernel, respectively. Then, the filtered version of each color channel is transformed back to CIEXYZ representation and thereafter to CIELAB. As a result, the representation of the image is called S-CIELAB, which includes both the spatial filtering and the CIELAB processing. Finally, the color difference between the S-CIELAB representation of two images is computed using the standard CIELAB color difference formula:

$$\Delta E^*_{ab} = \sqrt{(\Delta L^*)^2 + (\Delta a^*)^2 + (\Delta b^*)^2}, \quad (13)$$

where $\Delta L^* = L^*_o - L^*_h$, $\Delta a^* = a^*_o - a^*_h$, and $\Delta b^* = b^*_o - b^*_h$, and L^*_o, a^*_o, and b^*_o are the original continuous-tone images and L^*_h, a^*_h, and b^*_h are the halftone images in CIELAB (after going through S-CIELAB process and being converted back to CIELAB). Computation of ΔE^*_{ab} is a pixel-by-pixel operation and the color difference between two images is usually reported as the average ΔE^*_{ab} over all pixels. However, relying only on the average of S-CIELAB color difference values might not give us a complete insight to color reproduction error over images; therefore, we consider the maximum S-CIELAB color difference and S-CIELAB color difference greater than 5 units together with the average S-CIELAB in this work.

5. RESULTS

In this section, we study the impact of using a Gabor filter bank instead of Hough transform in improving the sharpness, structural similarity, color difference, and computation time. In our previous work [21], we used Hough transform in the preprocessing step, and found that by setting $k_1 = 1$ and $k_2 = 1.8$, halftone output achieves a desirable degree of sharpness enhancement and simultaneously improves the preservation of tonal and structural similarity. We used a test set including 20 images with different texture characteristics. Some of them are natural photographs and some are photographs of artworks such as oil paintings and sculptures. Links to access the test images are provided in Ref. [36]. The proposed algorithm and evaluations are implemented using Matlab.

As discussed in Section 3.2.2, to extend the monochrome structure-aware IMCDP to color halftoning, we used two approaches. In this section, we use the notation "*3CH*" to indicate that the orientation information of three channels have been processed separately, and "*1CH*" to indicate that orientation information has been extracted from the luminance component. We then evaluate the performance of the Gabor filter using fixed ($k_2 = 1.8$) and variable k_2 ($1.6 \leq k_2 \leq 2$) for one channel (1CH) and three channels (3CH) and compare them to the results obtained from the original IMCDP and Hough-based structure-aware IMCDP. In all the evaluations, we use Hough 1CH (the approach in our previous work [21]) as a baseline, and the reported blur, MSSIM, and S-CIELAB metrics for all images are normalized to those reference values for each image. This means that the normalized value of blur, MSSIM, and S-CIELAB of Hough 1CH is by definition 1 and it is illustrated as a dashed horizontal line in all reported graphs in this section.

5.1 *Sharpness*

As discussed in Section 4.2.1, we used the blur metric to study the sharpness of the results. Figure 3(a) illustrates the normalized blur metric for different approaches. The dashed line at 1 represents the reference method, which is using the Hough transform 1CH in the preprocessing step. The solid line inside each box shows the median of results for each approach. According to Fig. 3(a), regardless of using Hough transform or Gabor filter in preprocessing

step, the structure-aware versions of IMCDP overall result in lower blur metric, indicating sharper halftones, than the original IMCDP. Moreover, all the box plots corresponding to approaches using Gabor filter bank in preprocessing step lie under the Hough 3CH's box and the reference line, showing that Gabor filter banks approach outperforms Hough transform in extracting orientation information. Comparing boxes for 1CH and 3CH versions of each approach shows a similar median value (1CH have a slightly better increase in sharpness). However, bigger box length and whiskers for 1CH versions show that the results are slightly more dispersed compared to 3CH versions. It means that using the orientation information extracted from the luminance component for all three channels is an acceptable simplification. This could also be inferred by the shape of the box for Hough 3CH. Hough 3CH's box is a very small box with median close to the reference line, which represents the Hough 1CH results. The small box-length in Hough 3CH indicates that the overall results in Hough 3CH have a high agreement with that in Hough 1CH. In other words, using the orientation information extracted from the luminance component for all three channels is a reasonable approximation, but not a precise alternative solution.

5.2 *Structure Similarity*

As discussed in Section 4.2.2, MSSIM was used to evaluate the performance of the proposed method in preserving the structural similarity in halftone images. Fig. 3(b) represents the normalized MSSIM for different approaches. The dashed line at 1 represents the reference method, which is using the Hough transform 1CH in the preprocessing step. According to this figure, regardless of using Hough transform or Gabor filter banks in preprocessing step, the structure-aware IMCDP results in higher MSSIM, indicating that the structure-aware versions of IMCDP reproduce details and structures better than the original IMCDP. Moreover, all the box plots corresponding to approaches using Gabor filter bank in preprocessing step lie above the Hough 3CH's box and the reference line, showing that Gabor filter banks outperforms Hough transform in preserving structural similarity. Comparing boxes for 1CH and 3CH versions of each approach shows a slightly higher median value for 1CH approaches. However, the sections of 3CH boxes are more even compared to those of 1CH boxes.

Bigger box-length and whiskers for 1CH versions show that the results are slightly more dispersed compared to 3CH versions. The results for MSSIM also show that using the orientation information extracted from the luminance component for all three channels is a reasonable approximation, but not a precise alternative solution. Looking at boxes for Gabor 3CH with fixed and variable k_2 (i.e., Gabor 3CH $k_2 = 1.8$ and Gabor 3CH $1.6 \leq k_2 \leq 2$, respectively), one can observe that the box plot in Gabor 3CH has a higher median value, resulting in halftone with better preservation of structures.

We also did a further investigation regarding the outlier datapoints in Gabor 3CH $k_2 = 1.8$, Gabor 3CH $1.6 \leq k_2 \leq 2$, and Gabor 1CH $k_2 = 1.8$ in Fig. 3(a). The outlier datapoints in these box plots correspond to the same image. However, we did not observe the same image resulting in an outlier of MSSIM value in Fig. 3(b). This suggests that this outlier point could be derived from the nature of the image, and not the method.

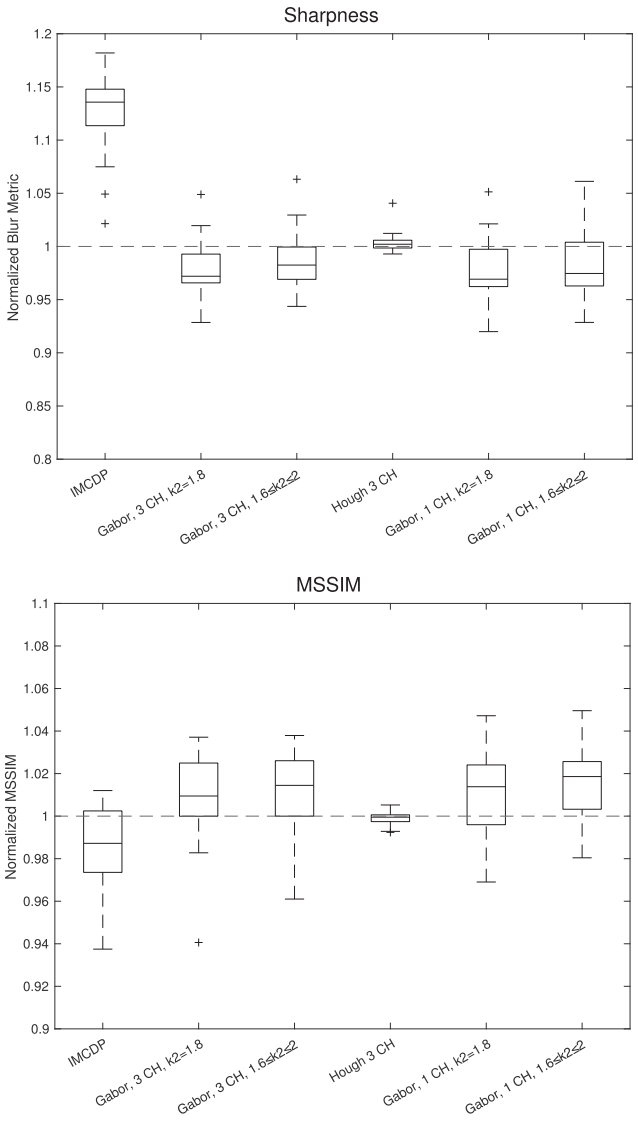

Figure 3. (a) Sharpness evaluation for different approaches according to normalized blur metrics. Lower blur metric indicates sharper halftones, (b) MSSIM evaluation for different approaches according to normalized MSSIMs. Higher MSSIM indicates more structural similarity. In both panels, dashed line at 1 represents the reference method (Hough 1CH).

5.3 *Color Difference*

As discussed in Section 4.2.3, we used S-CIELAB to evaluate the color reproduction error in our proposed method. Figure 4(a), (b), and (c) illustrates the results for average S-CIELAB, maximum S-CIELAB, and S-CIELAB>5, respectively. The dashed line at 1 represents the reference method, which is using the Hough transform 1CH in the preprocessing step. According to Fig. 4(a), the average color reproduction error in the original IMCDP is lower

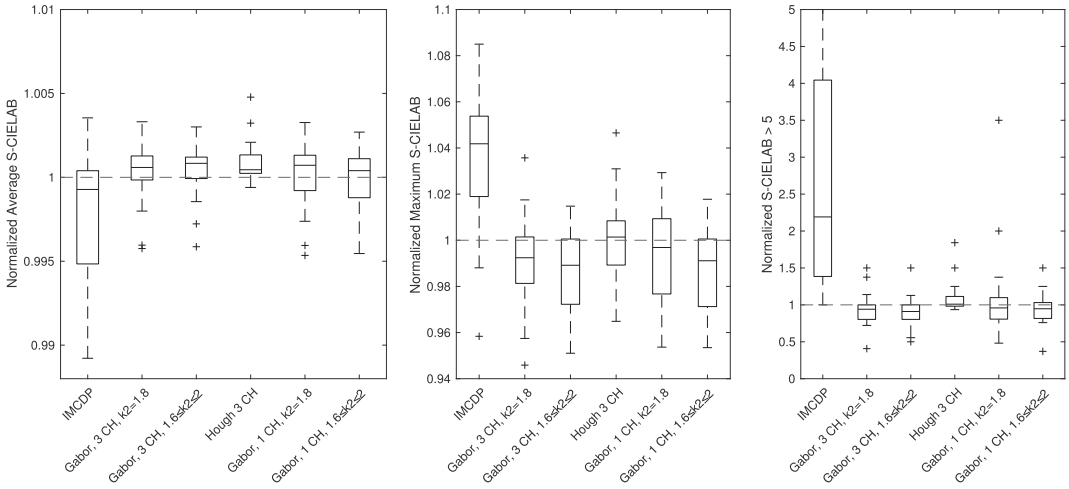

Figure 4. Color difference evaluation according to normalized S-CIELAB metrics, using the Hough 1CH's S-CIELAB metric as a measure of scale. (a) Average S-CIELAB (b) maximum S-CIELAB (c) S-CIELAB>5. The dashed line at 1 represents the reference method (Hough 1CH).

than the structure-aware versions of it, indicating better color reproduction in halftone outputs. However, relying only on the average of S-CIELAB values might not give us a complete insight to color reproduction error over images, therefore, we consider the maximum S-CIELAB and S-CIELAB>5 together with the average S-CIELAB. Comparing the maximum values of S-CIELAB in Fig. 4(b) indicates that the structure-aware versions of IMCDP result in smaller maximum values of S-CIELAB. When studying the color reproduction error, color differences exceeding 5 units are easily perceptible by our HVS, and according to Fig. 4(c), the original IMCDP reproduces more visible errors than the structure- aware versions of it. In addition, results in Fig. 4(b) and (c) show that the Gabor filter outperforms Hough transform in reproducing halftones with faithful colors, resulting in smaller maximum S-CIELAB and fewer color difference>5.

5.4 *Computation Time*

As discussed in Section 3, one of the contributions of this paper is using a faster and more flexible approach for obtaining the angle in the preprocessing step. The Hough-transform-based preprocessing can be prohibitively expensive as it has cubic complexity however, as IMCDP has a quadratic complexity, using a preprocessing approach with at most quadratic complexity makes the structure-aware IMCDP as fast as original IMCDP. We used a Gabor-based approach to obtain the local orientation information in preprocessing step. G Gabor filters of size $S \times S$ are generated only once and thereafter applied to images. As Gabor filters are applied by convolving the images with the filters, the complexity of calculating the response to one Gabor filter of size $S \times S$ at one pixel is $O(S^2)$. For an image with size $N \times N$, applying G Gabor filters on all pixels will be of $O(N^2 \times G \times S^2)$, which is quadratic in terms of the image size or linear in terms of number of pixels.

Figure 5 shows the result for preprocessing computation time. As can be seen in Fig. 5(a), using a Gabor-based approach in preprocessing step considerably decreases the computation time. Because the order of magnitude in computation time is different for Hough-based and Gabor-based approaches, we use Fig. 5(b) to clearly illustrate the computation time in Gabor-based approaches. The reported time is the average running time for three trials, and it is based on the current implementation of the proposed algorithm in Matlab on a MacBook Pro equipped with 2.6 GHz Intel Core i7 CPU and 16 GB 2400 MHz DDR4 memory.

Figures 6 and 7 represent visual examples of images in our dataset. As can be seen in Fig. 6, images being halftoned by the structure-aware IMCDP, Fig. 6(c) and (d), are perceived to be sharper than the image halftoned by the original IMCDP in Fig. 6(b). The structure-aware IMCDP reproduces both the details and structures and the color better than the original IMCDP. Structure-aware IMCDP performs better than the original IMCDP in displaying highly-detailed appearance and conveying feeling of 2.5D structural features present in a 2D image.

Fig. 7 illustrates a cropped region of "*Relief for the chapel*" at low resolution of 100 dpi to clearly demonstrate the individual dots and halftone structure in our proposed method. The original IMCDP and its structure-aware versions present pleasant and homogeneous halftone structures. Gabor 3CH with variable k_2 $(1.6 \leq k_2 \leq 2)$ in Fig. 7(b) and Gabor 1CH with variable k_2 $(1.6 \leq k_2 \leq 2)$ in Fig. 7(c) create sharper halftones compared to the original IMCDP in Fig. 7(a). Moreover, according to the evaluation metrics presented in Figs. 3 and 4, using the orientation information extracted from the luminance component for all three channels is acceptable approximation, but not a precise alternative. Visual comparison of Gabor 3CH in Fig. 7(b) and Gabor 1CH in Fig. 7(c) presents similar halftone structures and agrees with objective results that using only the luminance component to extract orientation information could be considered as a reasonable approximation.

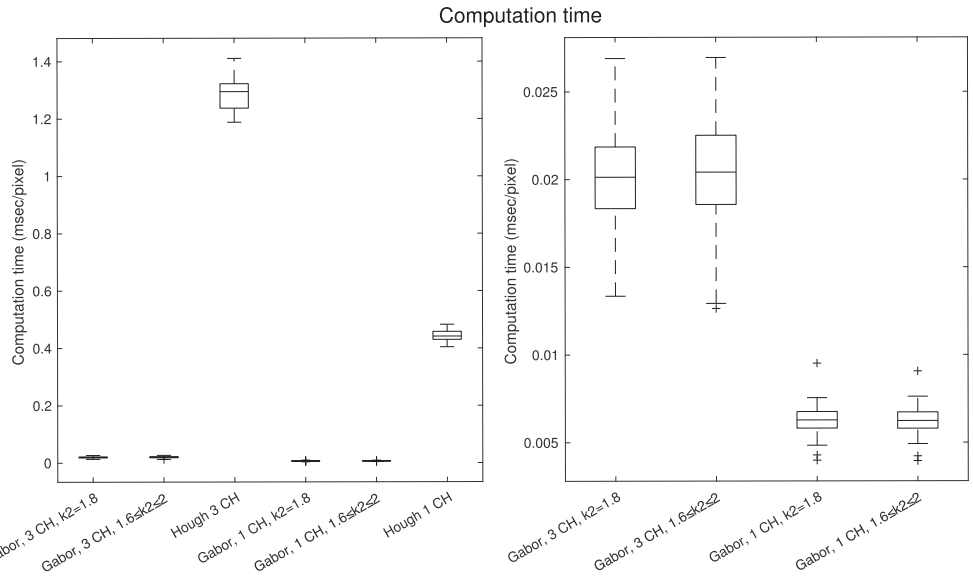

Figure 5. preprocessing computation time. (a) Comparison of all approaches (b) comparison of only Gabor-based approaches.

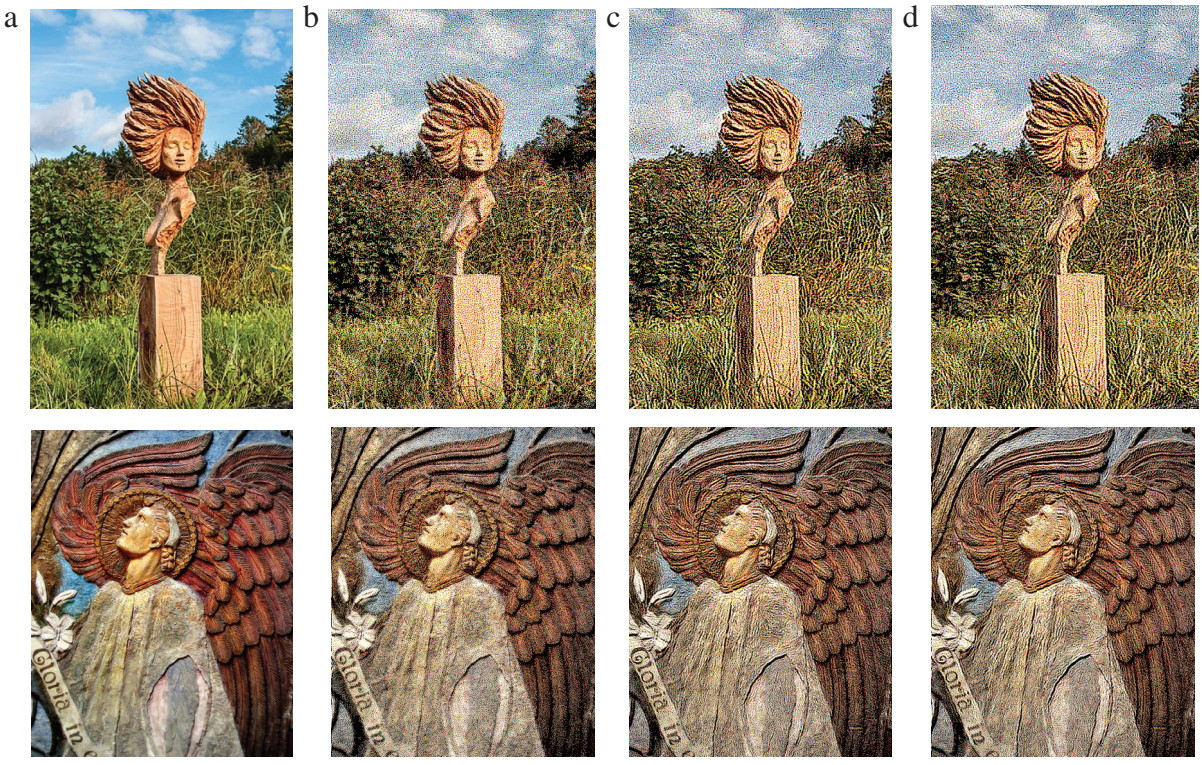

Figure 6. (a) Original continuous-tone image: top row "In the wind" [37], and bottom row "Relief for the chapel" [38]. (b) Halftoned image with original IMCDP, (c) Halftoned image with proposed color structure-aware IMCDP, Gabor 3CH with fixed $k_1 = 1$, $k_2 = 1.8$, (d) Halftoned image with proposed color structure-aware IMCDP, Gabor 3CH with $k_1 = 1$ and variable k_2 ($1.6 \leq k_2 \leq 2$). In (c) and (d), the orientation information is extracted from three different colorant channels C, M, Y, independently. Halftone images are displayed at resolution 200 dpi. The color version of this figure is best viewed in the electronic version of this paper.

6. CONCLUSION AND FUTURE WORK

The recently proposed structure-aware IMCDP improves the original IMCDP halftoning algorithm in terms of the reproduction of high-frequency details, structures, and tones by aligning the halftone structures with the dominant orientation of pixels in a neighborhood. However, Hough-transform-based preprocessing is computationally costly (cubic complexity), and sharpness enhancement is applied statically across the entire structured regions of the image. These limitations made the structure-aware version

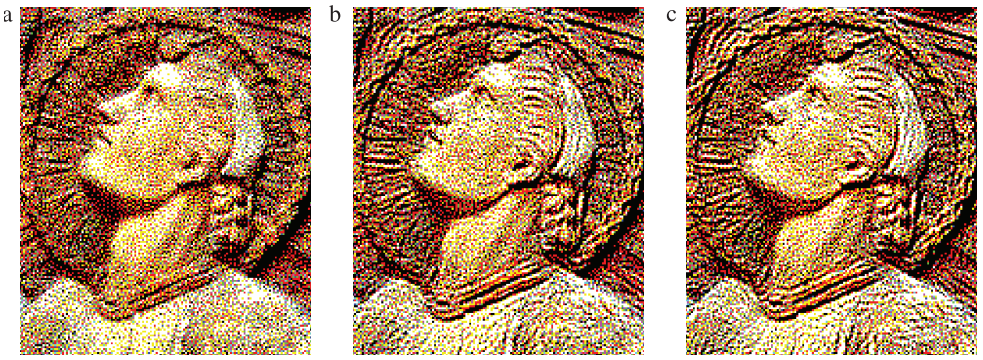

Figure 7. (a) IMCDP, (b) Gabor 3CH with variable k_2 ($1.6 \leq k_2 \leq 2$). The orientation information is extracted from three different colorant channels C, M, Y, independently. (c) Gabor 1CH with variable k_2 ($1.6 \leq k_2 \leq 2$). The orientation information is extracted from only the luminance channel. Halftone images are displayed at resolution 100 dpi. The color version of this figure is best viewed in the electronic version of this paper.

not suitable for larger images as larger images often contain variable sharpness and texture, and the size of the image can make the computation challenging. In this paper, we address both these limitations, and extend the method to color halftoning. We use a Gabor-based approach in preprocessing step that not only decreases the computation time by orders of magnitude (from cubic to linear) but also improves sharpness enhancement, structure similarity, and color consistency. Using the magnitude of Gabor responses to characterize texture and sharpness allows the method to have control over the degree of sharpness enhancement in different parts of an image. The adaptive adjustment of sharpness enhancement gives more flexibility to the user in improving the visual quality of image reproduction in our proposed structure-aware halftoning algorithm. In addition, we extend the method to color halftoning. We studied two approaches: extracting the structure information separately from each channel and applying them to color channels independently and using only the luminance channel structure information for all color channels. According to our investigation, halftoning each color channel based on its structure information produces more stable improvement for all image types; however, the objective evaluation and visual comparison of halftone structures show that the results are on average similar. In other words, the luminance orientation information is an acceptable approximation for orientation in different color channels, but it is not a precise alternative.

In this work, the performance of the structure-aware color halftoning has been validated using digital images. However, in printing color halftoned images, print settings such as print resolution, type of the printer, paper quality, etc. affect the print quality and appearance. To study the impact of print parameters on reproduction of image structures and details, we used a custom printer (screen printing) and validated the performance of the presented method [39].

Moreover, the proposed efficient adaptive structure-aware color halftoning can be extended to 3D halftoning to improve the reproduction of 3D printed surfaces. The original IMCDP algorithm has been extended to 3D domain in Ref. [40] and the effect of applying variable halftone structures based on the spatial information has shown that different halftone structures could be used to control the reproduction of details [24, 41]. As a next step, we are planning to develop an adaptive structure-aware 3D color halftoning algorithm, which has all the reproduction qualities of IMCDP while being aware of the color and geometry of the 3D object.

ACKNOWLEDGMENT

This project was funded by ApPEARS (Appearance Printing European Advanced Research School), the European Union's Horizon 2020 programme under the Marie Skłodowska-Curie grant agreement No. 814158.

REFERENCES

[1] D. L. Lau and G. R. Arce, *Modern Digital Halftoning* (CRC Press, Boca Raton, FL, 2018).
[2] R. Ulichney, *Digital Halftoning* (MIT Press, Cambridge, MA, 1987).
[3] R. W. Floyd and L. Steinberg, "An adaptive algorithm for spatial gray-scale," Proc. Soc. Inf. Disp **17**, 75–77 (1976).
[4] V. Ostromoukhov, "A simple and efficient error-diffusion algorithm," *Proc. 28th Annual Conf. on Computer Graphics and Interactive Techniques* (ACM, New York City, NY, 2001), pp. 567–572.
[5] B. Zhou and X. Fang, "Improving mid-tone quality of variable-coefficient error diffusion using threshold modulation," ACM Trans. Graph. **22**, 437–444 (2003).
[6] J. F. Jarvis, C. N. Judice, and W. H. Ninke, "A survey of techniques for the display of continuous tone pictures on bilevel displays," Comput. Graph. Image Process. **5**, 13–40 (1976).
[7] P. Stucki, "MECCA-a multiple-error correction computation algorithm for bi-level image hardcopy reproduction, IBM Thomas J," *Watson Research Division* (IBM Thomas J. Watson Research Center, New York City, NY, 1981).
[8] M. Analoui and J. P. Allebach, "Model-based halftoning using direct binary search," Human Vision, Visual Processing, and Digital Display III **1666**, 96–108 (1992).
[9] S. Gooran, "Dependent color halftoning: Better quality with less ink," J. Imaging Sci. Technol. **48**, 354–362 (2004).
[10] D. J. Lieberman and J. P. Allebach, "Efficient model based halftoning using direct binary search," *Proc. Int'l. Conf. on Image Processing* (IEEE, Piscataway, NJ, 1997), vol. 1, pp. 775–778.
[11] D. J. Lieberman and J. P. Allebach, "A dual interpretation for direct binary search and its implications for tone reproduction and texture quality," IEEE Trans. Image Process. **9**, 1950–1963 (2000).
[12] H. Li and D. Mould, "Contrast-aware halftoning," Comput. Graph. Forum **29**, 273–280 (2010).

[13] R. Eschbach and K. T. Knox, "Error-diffusion algorithm with edge enhancement," JOSA A **8**, 1844–1850 (1991).
[14] W. M. Pang, Y. Qu, T. T. Wong, D. Cohen-Or, and P.-A. Heng, "Structure-aware halftoning," *ACM SIGGRAPH 2008 Papers* (ACM, New York City, NY, 2008), pp. 1–8.
[15] J. Chang, B. Alain, and V. Ostromoukhov, "Structure-Aware Error Diffusion," TOG **28**, 1–8 (2009).
[16] L. Liu, W. Chen, W. Zheng, and W. Geng, "Structure-aware error-diffusion approach using entropy-constrained threshold modulation," Vis. Comput. **30**, 1145–1156 (2014).
[17] N. J. Kwak, S. P. Ryu, and J. H. Ahn, "Edge-enhanced error diffusion halftoning using human visual properties," *Proc. Int'l. Conf. on Hybrid Information Technology* (IEEE, Piscataway, NJ, 2006), Vol. 1, pp. 499–504.
[18] X. Li, "Edge-directed error diffusion halftoning," IEEE Signal Process. Lett. **13**, 688–690 (2006).
[19] H. S. Lee, K. K. Kong, and K. S. Hong, ""Laplacian based structure-aware error diffusion," *Int'l. Conf. on Image Processing* (IEEE, Piscataway, NJ, 2010), pp. 525–528.
[20] D. Li, T. Kiyotomo, T. Horiuchi, M. Tanaka, and K. Shigeta, "Texture-aware error diffusion algorithm for multi-level digital halftoning," J. Imaging Sci. Technol. **64**, 50410–50411 (2020).
[21] F. Abedini, S. Gooran, V. Kitanovski, and D. Nyström, "Structure-aware halftoning using the iterative method controlling the dot placement," J. Imaging Sci. Technol. **65**, 60404-1 (2021).
[22] P. V. Hough, "Method and means for recognizing complex patterns," U.S. Patent 3,069,654" (1962).
[23] S. Gooran and B. Kruse, "High-speed first- and second-order frequency modulated halftoning," J. Electron. Imag. **24**, 1–19 (2015).
[24] S. Gooran and F. Abedini, "3D surface structures and 3D halftoning," *Proc. IS&T Printing for Fabrication 2020* (IS&T, Springfield, VA, 2020), pp. 69–74.
[25] F. W. Campbell and J. G. Robson, "Application of Fourier analysis to the visibility of gratings," The J. Phys. **197**, 551 (1968).
[26] A. K. Jain and F. Farrokhnia, "Unsupervised texture segmentation using Gabor filters," Pattern Recognit. **24**, 1167–1186 (1991).
[27] G. Sharma and R. Bala, *Digital Color Imaging Handbook* (CRC Press, Boca Raton, FL, 2017).
[28] D. Shaked, N. Arad, A. E. Fitzhugh, and I. E. Sobel, "Color diffusion: error diffusion for color halftones," Proc. SPIE **3648** (1998).
[29] "RecommendationITU-RBT.601-7, Studio encoding parameters of digital television for standard 4:3 and wide-screen 16:9 aspect ratios," (2011).
[30] T. N. Pappas and D. L. Neuhoff, "Least-squares model-based halftoning," IEEE Trans. Image Process. **8**, 1102–1116 (1999).
[31] R. Näsänen, "Visibility of halftone dot textures," IEEE Trans. Syst. Man Cybern. **SMC-14**, 920–924 (1984).
[32] S. J. Daly, M. Rabbani, and C. T. Chen, "Digital image compression and transmission system visually weighted transform coefficients," US Patent 4,780,761, (1988).
[33] X. Zhang and B. A. Wandell, "A spatial extension of CIELAB for digital color image reproduction," J. Soc. Inf. Disp. **5**, 61–63 (1997).
[34] F. Crete, T. Dolmiere, P. Ladret, and M. Nicolas, "The blur effect: perception and estimation with a new no-reference perceptual blur metric," Proc. SPIE **6492**, 649201 (2007).
[35] Z. Wang, A. C. Bovik, H. R. Sheikh, and E. P. Simoncelli, "Image quality assessment: from error visibility to structural similarity," IEEE Trans. Image Process. **13**, 600–612 (2004).
[36] Links to test images. Accessed: Oct. 17, 2022.
[37] H. Haren, In The Wind. Accessed: Jun. 14, 2022.
[38] Kotomi, *Relief for the Chapel*. Accessed: Jun. 21, 2021.
[39] F. Abedini, A. Trujillo Vazquez, S. Gooran, and S. Klein, "Effect of halftones on printing iridescent colors," *Accepted for Presentation at the Color Imaging: Displaying, Processing, Hardcopy, and Applications Conf., at IS&T Electronic Imaging* (IS&T, Springfield, VA, 2023).
[40] F. Abedini, S. Gooran, and D. Nyström, "3D halftoning based on iterative method controlling dot placement," *Proc. IS&T Printing for Fabrication* (IS&T, Springfield, VA, 2020), pp. 69–74.
[41] F. Abedini, S. Gooran, and D. Nyström, "The effect of halftoning on the appearance of 3D printed surfaces," *47th Annual Conf. of Iarigai* (Iarigai, Darmstadt, Germany, 2021).

For information on reprints or reproduction contact
Donna Smith
Production Editor
The Journal of Imaging Science and Technology
Society for Imaging Science and Technology 7003
Kilworth Lane
Springfield, Virginia 22151 USA
703/642-9090 extension 107
703/642-9094 (fax)
jist@imaging.org
www.imaging.org